Nonlinear response in oligomers across chain lengths

Caroline Raepsaet,[1,*] Christiane Alba-Simionesco,[2] Cécile Wiertel-Gasquet,[1] and François Ladieu[1]
[1]Université Paris-Saclay, SPEC, CEA, CNRS, F-91191 Gif-sur-Yvette Cedex, France
[2]Université Paris-Saclay, LLB, CEA, CNRS, F-91191 Gif-sur-Yvette Cedex, France

(Received 11 July 2025; accepted 4 November 2025; published 2 December 2025)

We present third-order and first-order dielectric measurements on a series of N-propylene glycol (N-PG) oligomers, focusing on the role of molecular length N in the glass transition. To avoid polymeric effects, we restricted the study to short chains ($N = 1$–20). Linear dielectric susceptibility $\Delta\chi_1$ scales as $\frac{1}{N}$, suggesting that only the terminal hydroxyl (–OH) groups contribute significantly to the dipolar response, while the flexible backbone units remain largely inactive. Third-order susceptibilities $\chi_3^{(3)}$ exhibit a growing hump upon cooling for all N-PG, consistent with the Bouchaud-Biroli prediction. This allows us to extract the relative evolution of the number of dynamically correlated molecules $N_{\rm corr}$, which is as expected increasing upon cooling. But surprisingly, this evolution is identical across all oligomers, regardless of chain length, even though the size of the largest molecules likely exceeds that of the dynamic heterogeneities. This robustness of the relative evolution of $N_{\rm corr}(\tau_\alpha)$ allows to deduce that it is insensitive to the backbone linking the monomers, the fragility, the OH-bond density, or the strength of the dipole-dipole interactions among oligomers, standard criteria to describe the phenomenon. These findings challenge kinetically constrained models, which fail to account for the observed behavior, while supporting the predictions of the random first-order transition theory.

DOI: 10.1103/35b2-ysz4

I. INTRODUCTION

Despite a substantial spread of applications and the universal presence of glass in our modern environment, understanding the physics of the glass transition remains a challenge in solid-state physics and is still the subject of numerous studies [1–4] in the supercooled regime. If we cool down a glass-forming liquid, the viscosity increases, smoothly at the beginning then more and more quickly. At lower temperatures, a very small decrease of the temperature induces a huge increase of the viscosity [5,6] and of the structural relaxation time. At the glass transition temperature T_g, the liquid becomes so viscous that it can be considered, at the experimental timescale, as an amorphous, out of equilibrium solid: the glass. By convention, T_g is defined when the relaxation time is $\tau_\alpha = 100$ s, corresponding to a viscosity $\eta = 10^{11}$–10^{13} Pa s, depending on the value of the infinite-frequency shear modulus.

It is now well established that the relaxation of supercooled liquids is a nonhomogeneous phenomenon [5–7]. The material can be seen, at a given temperature, as a patchwork of small regions [8–10], the so-called dynamic heterogeneities (DHs). Inside a DH, the molecule dynamics are strongly correlated, but, as a first approximation, we can consider that the DHs are independent of their neighbors [6]. The total ensemble of DHs presents a wide dispersion of relaxation times and a narrower distribution of size. Mean values of size and relaxation time increase when the temperature decreases. Direct experimental evidence and study of DH have been presented long ago for granulars [3]. But in liquids, it would require the dynamic observation of every individual molecule, which is obviously not possible.

As we cannot observe directly the DH, indirect methods have been proposed and implemented [6]. Using the principles of dielectric spectroscopy [11], when a periodic electric field $\vec{E} = E_0 \cos(\omega t)$ is applied to a polar liquid, ω being the angular frequency and E_0 the amplitude, the polarization $\vec{P}$ of the liquid can be written [11] as

$$\vec{P} = \epsilon_0 \chi_1 \vec{E} + \epsilon_0 \chi_3 \vec{E}^3 + \epsilon_0 \chi_5 \vec{E}^5 + \cdots, \tag{1}$$

with ϵ_0 vacuum electric permittivity; χ_1, χ_3, and χ_5 dielectric susceptibilities at the order 1, 3, and 5; and $\vec{E}$ electric excitation field. Because of the symmetry $\vec{P}(-\vec{E}) = -\vec{P}(\vec{E})$, even terms are zero.

Bouchaud and Biroli (BB) [12] predicted that (1) the third-order dielectric susceptibility $|\chi_3|$ presents a large hump at an angular frequency $\omega_p \propto 1/\tau_\alpha$ and (2) the maximum of the hump is proportional to $N_{\rm corr}$, i.e., to the mean number of correlated particles in the DHs. The BB's prediction can be written as follows [12,13]:

$$\chi_3(\omega, T) \approx \frac{\epsilon_0\, \Delta\chi_1^2\, a^3}{k_B T} N_{\rm corr}(T)\, \mathcal{H}(\omega\tau_\alpha(T)), \tag{2}$$

with χ_3 dielectric susceptibility on the order of three, a^3 volume of a molecule, k_B Boltzmann constant, T temperature of the liquid, ω angular frequency of the electric field of frequency $f = \omega/(2\pi)$, and τ_α α-relaxation time of the liquid, $\Delta\chi_1 = \chi_1(\omega \to 0) - \chi_1(\omega \to \infty)$ with χ_1 linear dielectric susceptibility. $\mathcal{H}$ is a dimensionless unknown scaling

*Contact author: caroline.raepsaet@cea.fr

Published by the American Physical Society under the terms of the Creative Commons Attribution 4.0 International license. Further distribution of this work must maintain attribution to the author(s) and the published article's title, journal citation, and DOI.

function, which does not depend explicitly on the temperature (only indirectly through τ_α), and whose modulus shows a hump at a frequency f_p proportional to f_α, with $f_\alpha = \frac{1}{2\pi\tau_\alpha}$. Note that as the $\mathcal{H}$ function is quantitatively unknown, the absolute determination of $N_{\rm corr}$ remains extremely difficult [14]. However, the third-order dielectric susceptibility χ_3 for several temperatures gives access to the evolution of $N_{\rm corr}$ as a function of temperature [14]. Such measurements have already been made earlier for a large number of molecular systems, such as glycerol, propylene carbonate, 1-Propylene Glycol (1-PG), plastic crystals, to name a few [15–18]. Very recently a similar hump in the nonlinear shear-mechanical response was discovered [19] in two supercooled liquids (including 1-PG). This goes well with the key outcome of BB's theoretical prediction that any nonlinear response, as soon as it probes degrees of freedom coupled to the glass transition [12], gives direct access to the relative evolution of $N_{\rm corr}$ in temperature.

Despite these successes, BB's prediction is a matter of ongoing discussion in the literature, in particular about the existence of a direct link between χ_3 and $N_{\rm corr}$. On the theoretical side, the use, in the seminal BB's work [12], of a generalized fluctuation-dissipation relation was criticized and counter examples were looked after [20–22], but in the end they cannot be compared to BB's prediction as they do not fulfill $N_{\rm corr} \gg 1$, which is the key BB's assumption. On the phenomenological side, two distinct mechanisms contributing to χ_3 were elaborated—namely, the "absorption energy effect" [23,24] and the electrorheological effect [25]—and it was argued that they did not use any correlation length. It was however explained in Ref. [13] that the use of $N_{\rm corr}$ was implicit in the electrorheological effect and that this effect can be viewed as a particular mechanism consistent with BB's prediction. This allowed to physically reconcile the electrorheological effect with the two other phenomenological models—namely, the Toy model [26] and the Pragmatical model [27]—that had been elaborated independently in the mean time, and that are both explicitly consistent with BB's prediction. In other words, this explained [13] why all these phenomenological approaches yielded the same order of magnitude for χ_3. As for the "absorption energy effect," its reconciliation with all the other models was only achieved at the mathematical level—see the end of the Appendix of Ref. [13] and/or the Sec. 4.3 of the contribution of Albert *et al.* in Ref. [28]—by assuming the proportionality between $N_{\rm corr}$ and the quantity $N_{\rm corr,T}$ defined below in Eq. (8). This last step is only of mathematical nature, and this is the main reason why the consensus about the interpretation of χ_3 is not reached at present. A more in-depth discussion about the interpretation of χ_3 is given in Sec. IV.

In the present study, we focus on a family of oligomers, N-propylene glycol (N-PG), (OH−[C_3H_6−O]$_N$-H), see the schematic representations of the molecules in Fig. 1, and we vary N from 1 to 20. Starting from a single monomer, then increasing the size of oligomer chains, the spatial oligomer extension should be of the order of magnitude of DHs around the glass transition temperature T_g. Our main idea is to test, by dielectric linear and nonlinear (3ω) spectroscopy, whether there is, or not, an influence of the length of the molecule on the glass transition. If such an effect were to be revealed, this would give access to the size of DHs; if not, it would show

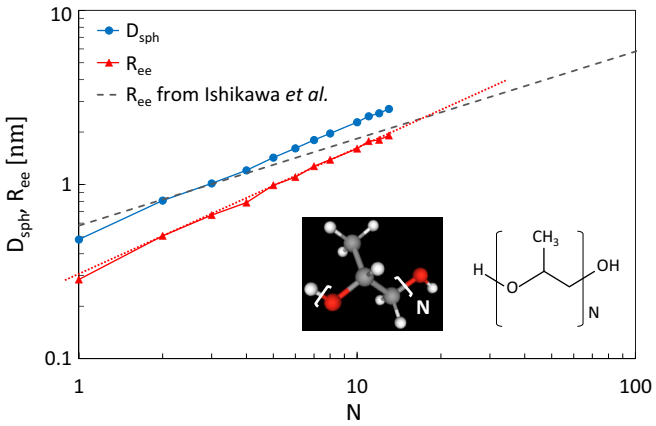


FIG. 1. Numerical simulations for various N-PG, with $N \leqslant 13$, of R_{ee}—red triangles—and of D_{sph}—blue dots. For each value of N, R_{ee} is the distance between the oxygen atoms of the two ending –OH groups. The dotted red line is a guide for the eye, corresponding to a slope $\gamma_R = 0.74$. The blue dots represent the diameter D_{sph} of the smallest sphere containing the molecule. The numerical uncertainties are of the order of the size of the dots. The black dotted line represents the extrapolation to our experimental range of R_{ee} reported by Ishikawa *et al.* [29] by using the experiments of Allen *et al.* [30] far in the polymer regime ($N > 10^3$). Representations of the N-PG molecule have been inserted: bottom left, oxygen, carbon and hydrogen atoms are, respectively, represented as red, gray, and white spheres; bottom right, SMILES of N-PG.

that DH relaxation does not depend on the backbone linking the monomers together. Whichever of these two possibilities turns out to be true, the experimental verdict will significantly deepen our understanding of the glass transition and constrain the few first-principles theories of this phenomenon so widespread in nature.

The paper is organized as follows: We first give an overview of the experimental conditions and justify our choice of N-PG. In the second part, we show the results of our measurements, obtained from the linear and nonlinear susceptibilities. Then, we discuss our results showing that the relative increase of $N_{\rm corr}(\tau_\alpha)$ is an extremely robust quantity since it is insensitive to many of the parameters used to characterize the various supercooled molecular systems. Finally, we critically discuss the main first-principles theories of the glass transition with respect to our data.

II. EXPERIMENTAL SETUP AND JUSTIFICATION OF THE CHOSEN RANGE IN N

A. Materials

1-PG and its oligomers (N-PG), HO−[C_3H_6−O]$_N$−H, form an interesting corpus [31,32]. In Fig. 1, schematic representations of the molecules have been insterted. With an –OH group at each end, the molecules are very polar (dipolar moment of 1-PG = 2.25 D) and therefore good candidates for dielectric measurements. Varying the value of N, we have a set of molecules with the same dielectric –OH contributors at both ends and a molecular length increasing with N. The series of N-PG that we studied are those available commercially, namely, 1-, 2-, 3-, 7-, 12-, and 20-PG: We bought 1-,

7-, and 12-PG from Sigma-Aldrich, 2- and 20-PG from Alfa Aesar, and 3-PG from ACROS ORGANICS. They were used as received.

B. Experimental setup

The third-order dielectric susceptibility $\chi_3^{(3)}$ was measured on the dedicated setup [14,33,34] developed earlier in our group in order to separate with a very good sensitivity the small third-order 3ω dielectric response from the main 1ω contribution, which is many orders of magnitude higher. In this setup, two pairs of stainless steel electrodes of diameter 20 mm and separated by Mylar® spacers are immersed in the liquid of interest. They form two samples of thicknesses 13 and 26 μm measured simultaneously in the same closed cell with a finely regulated temperature. The linear susceptibility $\Delta\chi_1$ of both samples is measured in the same configuration before and after every nonlinear measurement to verify the absence of crystallization. For each oligomer, 5–7 temperatures were measured close to T_g, in a frequency range 10^{-1} to 10^3 Hz.

When using such thin spacers, knowing precisely the actual value of the sample thickness e is difficult, since it may be affected by the presence of micrometric dusts that might increase the value of e. As this issue becomes negligible for large values of e, we performed additional linear measurements with samples 175 μm in thickness, on a Novocontrol Alpha-A broadband dielectric/impedance spectrometer. For each oligomer, experiments were done for 15 temperatures, in a frequency range 10^{-2} to 10^6 Hz, and a sample diameter of 20 mm. Thus, we were able to remove the uncertainties on the thickness of the thin samples.

C. Justification of the N range

1. Estimating a priori the relevant oligomer size

How can we be sure that choosing $N \leqslant 20$ guarantees that all our N-PG remain in the oligomer regime, i.e., avoid all the complexities arising in polymers such as entanglement, or reptation in transient tubes? A first indication comes from the works of Gainaru *et al.* [31,32] which indicates that, in N-PG, these complex effects take place only for $N \geqslant 90$. Besides, the onset of the polymeric behavior is also commonly defined as the value of N for which the chain conformation follows a random walk statistics, which is the case for $N \geqslant 30$ according to Ref. [32].

To be fully sure that we are not in the polymer regime, we have studied the evolution of the end to end distance R_{ee} in our molecules. As this is beyond any experimental sensitivity for such short molecules, molecular dynamics calculations is an efficient alternative. We used two open source codes: AmberMD [35] to prepare the input data (molecule geometry, force fields, box preparation,...) for OpenMM [36], which simulated the movement of the molecules.

In order to avoid excessively long stabilization and calculation times, the simulations have been made at high temperature, 450 K, i.e., well above T_g. This is substantially higher than the temperature range of our experiments, 175–220 K. However, the density weakly changes, no more than 5%−10% [37], between 450 K and T_g. It is therefore valid to approximate the average geometric features around T_g, e.g., the end to end distance of the molecules, by those calculated at 450 K.

For each oligomer, N ranging from 1 to 13, OpenMM was run to simulate the movement of 50 molecules. We check that the system has reached the equilibrium in our simulations by studying the dipole-dipole correlation function $C(t)$. Starting by design from $C(t=0)=1$, when t increases, each dipole decorrelates from its initial orientation; thus, $C(t)$ decreases to zero. The system is equilibrated when all the dipoles have relaxed, then we have $C(t)=0$. After equilibration, the MD calculation is extended for 4000 ps. For each time interval of 4 ps, we calculated for every molecule (1) the distance end to end, R_{ee}, between the oxygen atoms of the two ending –OH groups, and (2) the diameter of the smallest sphere containing the molecule D_{sph}. Figure 1 presents the evolution of R_{ee} and D_{sph}, averaged on time and molecules, as a function of N. Both quantities follow a power law of N, as we detail now.

In Fig. 1, we can see that in our N range, D_{sph} is significantly larger than R_{ee}. This means that, as soon as $N=1$, the molecules are not forming a straight line between both ends. Increasing N up to 13, from Fig. 1 one draws $R_{ee} \propto N^{\gamma_R}$, where $\gamma_R = 0.74 \pm 0.04$ is directly related to the effective dimensionality $d_{eff} \equiv 1/\gamma_R$. This shows that $R_{ee}(N)$ has not yet reached the standard value $\gamma_R = 0.5$ typical of the polymeric regime—corresponding to $d_{eff}=2$. More quantitatively, at 320 K, one can use the viscosity and light-scattering experiments made for a number of fractionated N-PG samples in a theta solvent [30], which were fairly well accounted for by the calculations of conformational energies made by using classical torsional and nonbonded interaction potentials in Ref. [29]. Performed in the range $10^3 < N < 10^4$, these experiments yield $R_{ee} = \sqrt{C_\infty n l^2}$, where $C_\infty = 5.05$, $n = 3N$ is the number of covalent bonds in a molecule of N-PG, composed of N monomers of three covalent bonds, and $l = 0.15$ nm is the mean length of the covalent bonds in our molecules. Thus, the relationship becomes $R_{ee} = \sqrt{N} \times 0.58$ nm. Accordingly, Fig. 1 reports the result of Ishikawa *et al.* [29] as a black dotted line extrapolated down to $N=1$ to meet our experimental range. By extrapolating our numerical results slightly above $N=13$, we see that our calculations intersect Ishikawa's result for a characteristic value of N given by $N_{\to polym} \approx 15-20$. This crossover value is close to the value of 30 that we anticipated, by using Ref. [32], for the oligomer to polymeric transition. This establishes that no polymeric effects are expected in our experimental results, except for $N=20$, as shown in Sec. III D. Finally, one observes in Fig. 1 that $D_{sph} \propto N^{\gamma_D}$, with $\gamma_D < \gamma_R$ since there is a trend for D_{sph}/R_{ee} to decrease slowly when N increases. This shows that the compactness of the N-PG molecules increases slowly with N in our selection range. This happens before the crossover that one expects for $N > N_{\to polym}$ toward the standard random walk characterized by $\gamma_R = 1/2$ as in the standard polymer regime of Ref. [30].

2. Comparison of R_{ee} to D_{corr}

Thanks to our numerical simulations, we can translate the value of N in terms of typical spatial size $\mathcal{L}(N)$ of a molecule, namely, the end-to-end distance R_{ee} or the diameter D_{sph} of the smallest sphere embedding a molecule of N-PG. From

Fig. 1, we draw $\mathcal{L}(N) = q a_{\rm mono} N^{\gamma_{\rm R}}$, where $a_{\rm mono} = 0.5$ nm is the length of a monomer, $q = 0.6$ for $\mathcal{L}(N) \equiv R_{\rm ee}(N)$ and $q = 1.0$ for $\mathcal{L}(N) \equiv D_{\rm sph}(N)$. We neglect the tiny difference between $\gamma_{\rm R}$ and $\gamma_{\rm D}$. As explained in Sec. II C 1, one has $R_{\rm ee} \propto N^{\gamma_{\rm R}}$ with $\gamma_{\rm R} = 0.74 \pm 0.04$. This corresponds to an effective dimensionality $d_{\rm eff} \equiv 1/\gamma_{\rm R}$, yielding $d_{\rm eff} \simeq 1.35$; i.e., our oligomers are more tortuous than just a straight line (where one would have $d_{\rm eff} = 1$) and much less compact than spherical objects (where one would have $d_{\rm eff} = 3$). This contrasts with the shape of DH's which, close to $T_{\rm g}$, have been evidenced in Ref. [38] to be compact, i.e., to have an effective dimensionality of 3. As a result, for a given T, there is an interesting crossover $N^\star$, where $\mathcal{L}$ equals the diameter $D_{\rm corr}$ of a typical dynamical heterogeneity. As $D_{\rm corr}$ slowly increases upon cooling, this crossover $N^\star$ depends on T, or equivalently on τ_α. The physical meaning of this crossover is the following: for $N < N^\star(\tau_\alpha)$ most of the N-PG molecules belong to only one DH, while whenever $N \geqslant N^\star(\tau_\alpha)$ any given molecule of N-PG spans over more than one DH.

To get an expression of $N^\star(\tau_\alpha)$, we write $N_{\rm corr} = \phi \times (D_{\rm corr}/a_{\rm mono})^3$ where $\phi \simeq 0.74$ is the maximal filling factor for assembly of $3d$ spheres. This implies that when discussing Eq. (3), the value of $N_{\rm corr}$ is given in terms of $a_{\rm mono}$, which in the case of oligomers represents a monomer, but in the case of a short molecule—such as glycerol—represents the whole molecule. As we shall see below, the experimental data about the absolute value of $N_{\rm corr}$ are broadly dispersed, but as they are given at $T_{\rm g}$, i.e., for $\tau_\alpha = 100$ s, we take into account, see Sec. III F, that $N_{\rm corr}(\tau_\alpha = 10\,{\rm ms}) \simeq 0.6 \times N_{\rm corr}(\tau_\alpha = 100\,{\rm s})$ to get the expression $N^\star(10\,{\rm ms})$ corresponding to the center of our range in τ_α of our 3ω experiments. Equating $\mathcal{L}(N^\star)$ with $D_{\rm corr}$ at $\tau_\alpha = 10$ ms, we get

$$N^\star(\tau_\alpha = 10\,{\rm ms}) = \left[\frac{0.6}{\phi\, q^3} N_{\rm corr}(\tau_\alpha = 100\,{\rm s})\right]^{\frac{1}{3\gamma_{\rm R}}} = (0.9 \text{ to } 1.8) \times [N_{\rm corr}(\tau_\alpha = 100\,{\rm s})]^{0.45} \tag{3}$$

where we have obtained the last equality by using the above-mentioned values for ϕ, $\gamma_{\rm R}$ and where the two values of the prefactor correspond, respectively, to $q = 1$ and to $q = 0.6$.

We now come to the values of $N_{\rm corr}(\tau_\alpha = 100\,{\rm s})$ reported in the literature, which appear quite dispersed, for the reasons that we shortly discuss now:

(1) $N_{\rm corr}(\tau_\alpha = 100s)$ might strongly depend on the considered glassformer: for example, by using the 4D-nuclear magnetic resonance technique [39,40], one finds that a typical DH contains 10 molecules for glycerol and 100 monomers for polyvinyl acetate.

(2) for a given glassformer, such as glycerol, the value deduced for $N_{\rm corr}(\tau_\alpha = 100\,{\rm s})$ strongly depends on the kind of experiment [39–41]: By using, e.g., the heat capacity spectroscopy data by extrapolating the Donth's group model, one finds from Ref. [39] that 100 molecules of glycerol are contained in a typical DH at $T_{\rm g}$, different from the value of 10 obtained with nuclear magnetic resonance [39,40].

(3) the random first-order transition theory (RFOT) estimate [3] is $N_{\rm corr}(\tau_\alpha = 100\,{\rm s}) \simeq 43$ for glycerol, which has a molecular fragility, a molecular weight and a dielectric susceptibility $\Delta\chi_1$ close to those of 1-PG. Of course, the OH-bond density is clearly different in 1-PG and in glycerol, but since we shall show in Sec. IV A 3 the irrelevance of this density the comparison of those two liquids is still justified to get an estimate of $N_{\rm corr}(\tau_\alpha = 100\,{\rm s})$.

(4) To our knowledge, the largest value ever reported in the literature comes from the field of polymers [42,43] stating that typically 1000 monomers lie within a DH at $T_{\rm g}$. However this extremely large value may be obscured by the quite involved microscopic phenomena that may arise in polymers, due to the complexity inherent to these so long molecules [44].

Consider first the latter value $N_{\rm corr}(\tau_\alpha = 100\,{\rm s}) = 1000$ inferred from polymer studies. By choosing the smallest possible value $q = 0.6$, i.e., by comparing $R_{\rm ee}$ and $D_{\rm corr}$, we obtain the top extreme value $N^\star(\tau_\alpha = 10\,{\rm ms}) \simeq 41$, which is clearly longer than our longest oligomer ($N = 20$). By comparing $D_{\rm sph}$ and $D_{\rm corr}$, i.e., by using $q = 1.0$, one gets $N^\star(\tau_\alpha = 10\,{\rm ms}) \simeq 20.5$, which (nearly) corresponds to our longest oligomer.

Moving to the former cases where the estimates of $N_{\rm corr}$ are taken from studies of small molecules, we get $2.6 < N^\star(\tau_\alpha = 10\,{\rm ms}) < 15$ depending on the value of q and $N_{\rm corr}(\tau_\alpha = 100\,{\rm s})$ one considers in the above-discussed interval—in Sec. IV B we shall determine $N^\star$ within RFOT. Overall, the fact that, apart from the top extreme case, $N^\star$ lies within our experimental range, or hardly above it, justifies our choice of our N range. As explained in the introduction, inspecting whether or not there is some N dependence for the relative evolution of $N_{\rm corr}$ in τ_α will either reveal the absolute size of the DH's close to $T_{\rm g}$, or show that the oligomer backbone does not have any effect on the growth of the DH's size in τ_α.

III. RESULTS

A. Linear measurements

The results of the linear dielectric measurements are presented for 3-PG in Fig. 2. We obtained similar qualitative results for the other oligomers. The range of temperatures has been chosen to be somewhat larger than the one over which χ_3 data are available, i.e., temperatures ranging from 196 to 220 K.

As expected, the loss contribution $\epsilon''(f)$ shows a large hump corresponding to the α-relaxation process, Fig. 2(a), whose maximum decreases slightly and shifts to higher frequency when the temperature increases. We define $f_\alpha = \frac{1}{2\pi\tau_\alpha}$ as the frequency corresponding to the peak, as shown in Fig. 2(a), an arrow pointing out f_α for $T = 196$ K.

The dielectric constant $\epsilon'(f)$, Fig. 2(b), presents a plateau at low frequency. When the temperature increases, the plateau extends to higher frequencies and its height lowers. Then, it decreases toward $\epsilon'(\infty)$, independent of T, measured at lower temperatures, nonrepresented in Fig. 2.

We use the phenomenological formula of Vogel-Fulcher-Tammann [45–47] (VFT) to fit the temperature dependence of the α-relaxation time:

$$\langle\tau_\alpha\rangle = \tau_0 \exp\left(\frac{DT_0}{T - T_0}\right), \tag{4}$$

where T_0 is the Vogel-Fulcher-Tammann temperature at which τ_α is supposed to diverge, D is the strength parameter, and τ_0 is the relaxation time at high temperature.

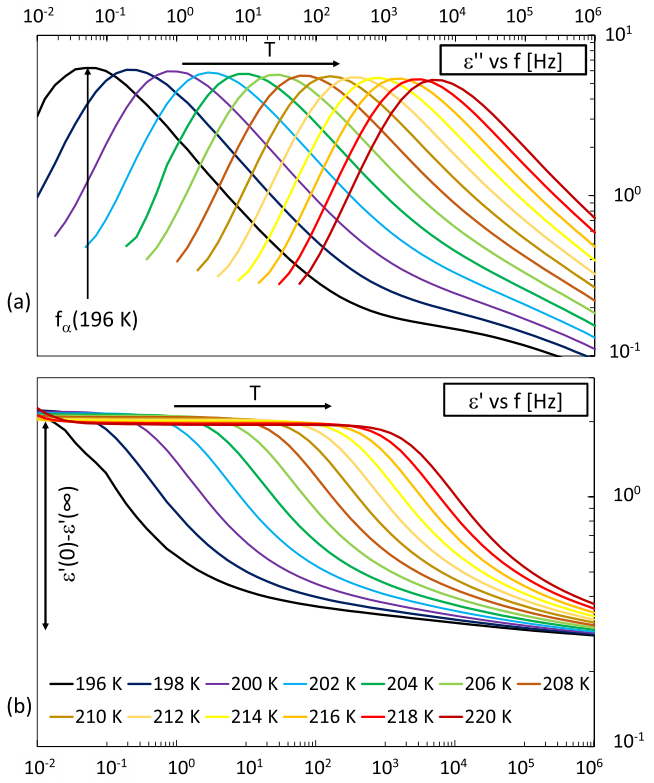


FIG. 2. Imaginary and real parts of the dielectric permittivity of 3-PG, measured on the Novocontrol spectrometer for temperatures ranging from 196 to 220 K: (a) ϵ'' and (b) ϵ' as a function of f (Hz).

We calculated also the fragility, commonly defined by [6]

$$m = \left.\frac{d(\log_{10}\tau)}{d(T_g/T)}\right|_{T_g}. \quad (5)$$

Table I summarizes the α-relaxation parameters of the VFT fit D, T_0, $-\log_{10}(\tau_0)$, the glass transition temperature T_g corresponding to $\tau_\alpha = 100$ s, and the fragility m. Overall our parameters are consistent with the previous studies existing in the literature such as in Refs. [31,32,48–50]. All this parameters present significant variations for the lower values of N, namely, 1–3, and very weak variations above. This smooth dependence on the chain length is also observed in the case of very flexible polymer chains, such as polyisobutylene, with a nonfragile behavior as T_g is approached [51].

TABLE I. Relaxation parameters of N-PG.

N	D	T_0 (K)	$-\log_{10}(\tau_0[\mathrm{s}])$	T_g (K)	m
1	16.8	115	13.9	168	51
2	10.9	150	13.8	195	69
3	9.9	150	13.7	191	73
7	8.1	160	13.3	197	82
12	8.7	160	13.9	198	82
20	9.1	160	14.3	199	84

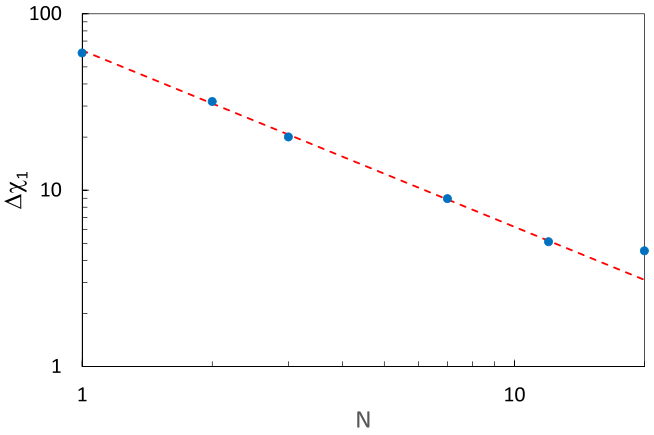


FIG. 3. Linear static susceptibility $\Delta\chi_1$ vs N, number of monomer units in the oligomer. The red dashed straight line has a slope -1 and is a guide for the eye. Blue dots are experimental results at temperatures corresponding to $f_\alpha \approx 10$ Hz ($\tau_\alpha \approx 15$ ms). The relative uncertainty on $\Delta\chi_1$ is on the order of the size of the points.

B. Static linear dielectric susceptibility

As $\epsilon = \chi_1 + 1$, the linear dielectric susceptibility $\Delta\chi_1$ is equal to the amplitude of the sample permittivity between $f \to 0$ and $f \to \infty$ [see Fig. 2(b)]:

$$\Delta\chi_1(T) = \Delta\epsilon(T) = \epsilon(f \to 0, T) - \epsilon(f \to \infty). \quad (6)$$

Figure 3 presents a log-log plot of the linear susceptibility $\Delta\chi_1$ measured for 1-, 2-, 3-, 7-, 12-, and 20-PG as a function of N, the number of monomers in the oligomer, at temperatures chosen to correspond to $f_\alpha \approx 10$ Hz ($\tau_\alpha \approx 15$ ms) (similar results have been obtained at other frequencies). The blue dots are the experimental points. A red dashed line of slope -1 has been drawn on as a guide for the eye: It shows that the experimental behavior is very close to $\Delta\chi_1 \propto \frac{1}{N}$. Theoretically, $\Delta\chi_1$ is given [11] by

$$\Delta\chi_1 = \frac{\mu^2(N) g_K(N)}{3\epsilon_0 N a^3_{\mathrm{mono}} k_B T}, \quad (7)$$

with $\vec{\mu}(N)$ the molecular dipole vector of N-PG and $g_K(N)$ the molecular Kirkwood factor expressing the static average correlations between dipoles. In Eq. (7), we have used the fact that the molecular oligomer volume is extremely close to $N a^3_{\mathrm{mono}}$ since the density—at room temperature—is mainly independent of N. As we shall show below—see Sec. III D—it may happen that $g_K(N)$ decreases as N increases, from $g_K(N=1) \simeq 2.85$ to $g_K(N=20) \simeq 1$. However, this is a much smaller variation than the 15-fold effect observed in Fig. 3. Taking into account these estimates of g_K gives $\mu(N=20) \simeq 1.69\mu(N=1)$, whereas assuming g_K being constant in N would yield $\mu(N=20) = \mu(N=1)$. Anyhow, $\mu(N=20)$ and $\mu(N=1)$ are surprisingly close one to another, as if the main contribution to the linear susceptibility would come from the two –OH end groups, while the other chemical units of the chain have no significant influence on $\Delta\chi_1$. This is a counterintuitive result, because the chemical units situated along the chain between the –OH groups have dipoles that are not that smaller than the –OH ending ones. On the other hand,

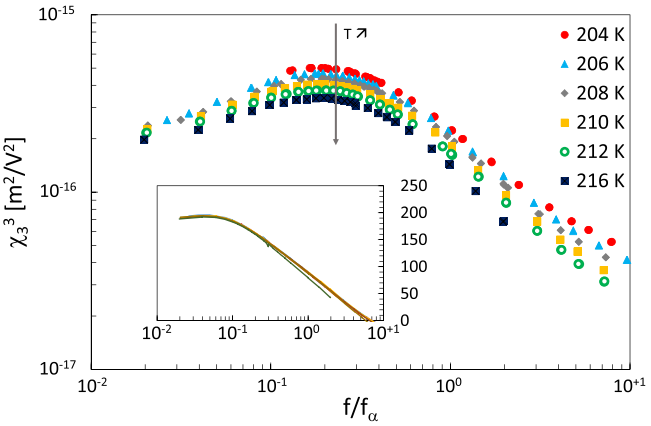


FIG. 4. Modulus of the 2-PG third-order susceptibility, $|\chi_3^{(3)}|$ vs $\frac{f}{f_\alpha}$, where f_α is the α-relaxation frequency (see text). The maximum of the peak is decreasing when the temperature increases. In the insert, we present the phase of $\chi_3^{(3)}$ (deg), which turns out to collapse into a temperature independent master curve. The relative uncertainty on $\chi_3^{(3)}$ is on the order of the size of the points.

this suggests that in this system, changing the length of the molecule does not perturb the dipoles that dominate the dielectric linear response. This may be viewed as an unexpected asset of the *N*-PG series that may simplify the analysis of the *n*-linear response, to which we move now.

C. Third-order susceptibility

The modulus of the third-order dielectric susceptibility at 3ω is presented in Fig. 4 for 2-PG as a function of $\frac{f}{f_\alpha}$, with the usual definition of the relaxation frequency $f_\alpha \equiv \frac{1}{2\pi\tau_\alpha}$. Similar results were obtained for the other oligomers. The shape of the curves in frequency, as well as their evolution with the temperature, are in good agreement with Bouchaud-Biroli's predictions made in Refs. [12,38] and further commented in Refs. [33,52]:

(1) For any given temperature, $|\chi_3^{(3)}(\frac{f}{f_\alpha})|$ shows a large hump around $f_p \simeq 0.2 f_\alpha$, which can be understood as follows. At low frequency $f < f_p$, the probing time $t_{pr} \propto 1/\omega$ associated with the electric field is much longer than τ_α. Thus, the system significantly relaxes during t_{pr} and flows to other configurations: As a result, $\chi_3^{(3)}$ will decrease to the liquid trivial contribution corresponding to effectively independent molecules. In contrast, at high frequency $f \gg f_p$, the probing time t_{pr} is much smaller than τ_α, and the system typically does not have enough time to relax, except in the fastest DHs, which become fewer and fewer as frequency increases. Hence in this solid like situation, $\chi_3^{(3)}$ decreases when f increases. Between these two extremities, i.e., whenever $t_{pr} \approx \tau_\alpha$ we have an important dielectric response with a maximum for $f = f_p$. Given the spread of the $\chi_3^{(3)}$ data, the value of f_p was obtained using a polynomial fit of the experimental curve around the peak. The resulting uncertainty interval is $f_p \times (1.0 \pm 0.073)$.

(2) The maximum of the peak is decreasing when the temperature increases: We will see in Sec. III F that from this behavior in temperature, one can deduce by which amount the number N_{corr} of dynamically correlated molecules decreases when heating up the sample.

(3) In the insert of Fig. 4, we see that as predicted by Eq. (2), the phase of $\chi_3^{(3)}$ collapses onto a master curve in $(\frac{f}{f_\alpha})$.

As further discussed below, all the features of Fig. 4 are consistent with those reported on simple glass forming liquids, such as in Refs. [14–16,33,54,55].

D. N dependence of the first- and third-order spectra

In Fig. 5, we compare the shape in frequency of the linear and nonlinear responses of the various *N*-PG. We have, for each value of *N*, chosen a temperature for which $f_\alpha \approx 10$ Hz, so that the α relaxations are comparable. Figure 5(a) shows a broadening of the peak of χ_1'' when *N* increases. To highlight this phenomenon, we show in the lower part of Fig. 5(a) the log-log slope of χ_1'' in $\frac{f}{f_\alpha}$, slope $= \frac{\partial \log(|\chi_1''|/|\chi_1''|_p)}{\partial \log \frac{f}{f_\alpha}}$. This broadening of the peak of χ_1'' with *N* deserves some comments:

(1) On the left part of the peak, two distinct frequency dependencies can be distinguished. In the first group, $N = 1$–7, the shape of the peak is that of short molecular glass formers: Increasing frequency from the lowest values of f/f_α, one first encounters the regime dominated by the dc conductivity $\chi_1'' \propto f_\alpha/f$, before the dipoles take the leading role, yielding $\chi_1'' \propto f/f_\alpha$ as expected from the fluctuation-dissipation theorem. This standard behavior progressively changes when increasing *N*, the broadening of the peak being perceptible for $N = 12$ and much more visible for $N = 20$. As explained in Ref. [32], this deformation is due to the emergence of a normal mode, i.e., to the dielectric contribution coming from the dielectric dipole μ_{chain} summed up all along the chain of each *N*-PG molecule. This normal mode contribution appears and grows with *N* and our results depicted above are in good agreement with Refs. [32,48], which, for $T \geqslant T_g$, reported a normal mode deformation of the α-relaxation peak for $N \geqslant 17$.

(2) On the right side of the peak of χ_1'', the absolute value of the logarithmic slope decreases with *N*, especially between 1-PG and the other *N*-PG. On general grounds, this amounts to an increase with *N* of the width of the distribution of the relaxation times [11], which is not surprising owing to the increase of the complexity of the system with *N*. Another complementary interpretation, which is more specific to the dielectric linear susceptibility, can be found in the recent works of Blochowitz's group [53] showing that the larger the Kirkwood factor g_K, the steeper the slope $-\beta_{diel}$ of χ_1'' on the right flank of the α peak (see Fig. 5 for a precise definition of β_{diel} commonly associated with the streching of the relaxation). This comes from the fact that dielectric responses are generically made of a "self" and a "cross" part reflecting, respectively, the correlation of a given dipole with itself and with other dipoles [53,56]. References [53,56] have shown that the cross part increases in magnitude with the Kirkwood correlation factor g_K. Hence, there is a systematic β_{diel} variation in g_K since the dielectric cross part is steeper in frequency than the self part. For $N = 1$, Ref. [53] gives $g_K \simeq 2.85 \pm 0.15$ and $\beta_{diel} \simeq 0.67 \pm 0.02$, which is consistent with our findings in Fig. 5(a). In Fig. 5(a), we observe that β_{diel} decreases when *N* increases, converging to

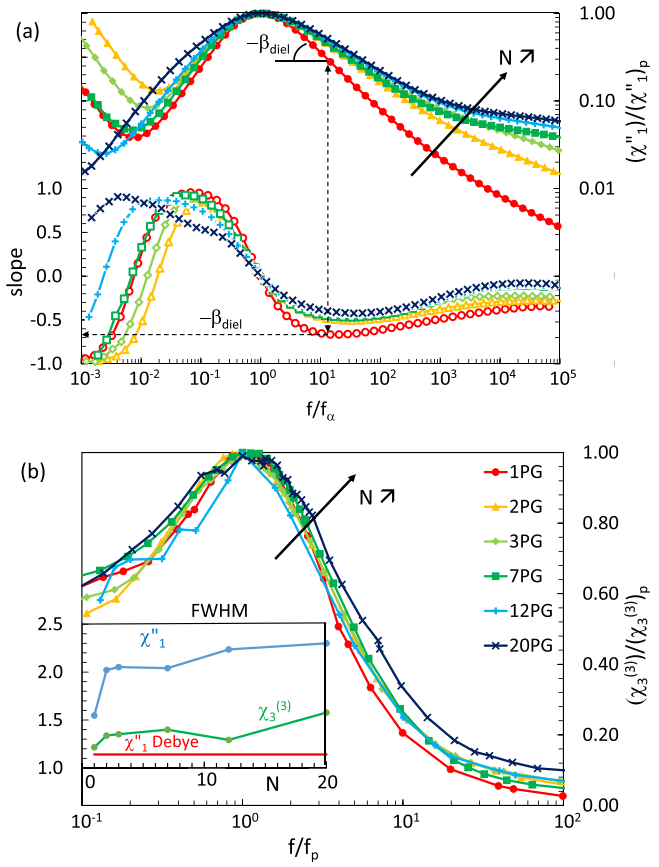


FIG. 5. Comparison of the linear and nonlinear measurements for the different values of N. Temperatures have been chosen so that $f_\alpha \approx 10$ Hz (see Table II). (a) The upper graph represents—right axis—the linear dielectric loss χ_1'' normalized to its peak. The lower part—left axis—is the log-log slope of the upper curves, i.e., the logarithmic derivative of χ_1'' with respect to $\log \frac{f}{f_\alpha}$, slope $= \frac{\partial \log(|\chi_1''|/|\chi_1''|_p)}{\partial \log \frac{f}{f_\alpha}}$. For the high-frequency flank of the α peak, i.e., for frequencies $f > f_\alpha$, the absolute value of this slope reaches its maximum—called β_{diel} in the main text [53]—for $f \approx 20 f_\alpha$. At high frequency, the shape of the curves and their discrepancies are difficult to interpret due to the potential contribution of β or secondary relaxation modes. As they have no influence on our results, concerning lower frequencies, we will not discuss them. (b) Module of the third-order dielectric susceptibility at 3ω, $|\chi_3^{(3)}(\frac{f}{f_p})|$, normalized by the peak value—right axis. In the insert, we compare the evolution of the FWHM for a Debye relaxation, χ_1'' and $\chi_3^{(3)}$—left axis.

TABLE II. Reference temperatures used to calculate the relative evolution of N_{corr}, with the corresponding values of f_α and τ_α within the same decade.

N	T_{ref} (K)	f_α (Hz)	τ_α (ms)
1	183	11	15
2	208	8	21
3	203	15	11
7	208	13	12
12	207	8	21
20	208	6	25

$\beta_{\text{diel}} \simeq 0.48 \pm 0.05$ for our largest N's. According to Fig. 1 of Ref. [53], this would correspond to a decrease of g_K to values close to 1 corresponding to mainly noninteracting dipoles at large N. For $N > 1$, we cannot really derive the value of g_K as we do not precisely know which dipoles are relevant for $\Delta\chi_1$ and which ones self average to zero. However, in the scenario above mentioned where the only relevant dipoles are the OH ones, one would easily anticipate that $g_K \to 1$ at large N, since the probability of having neighboring OH dipoles tends to zero for our longest oligomers.

Figure 5(b) shows the module of the third-order dielectric susceptibility at 3ω, $|\chi_3^{(3)}(\frac{f}{f_p})|$, normalized by the peak value. Overall, we notice very similar behaviors for χ_1'' and $|\chi_3^{(3)}|$: broadening of the hump when N increases, 1-PG curve separated from the other ones. A global analysis of the right side of the peak in Fig. 5(b) shows the same trends as for Fig. 5(a), namely, that the 1-PG curve is the narrowest, the 20-PG is the widest. This is understandable because the arguments given above for the linear response still hold qualitatively for the cubic response (for the self and cross parts in cubic responses, see the explicit simulations of Ref. [57]). Finally, the only difference between first- and third-order spectra above f_α is that the intermediate values of N are more closely packed for $|\chi_3^{(3)}|$ than for χ_1''.

A more local analysis close to the maximum of the peaks can be done by computing the so called full width at half maximum (FWHM) and compare it to the case of a pure Debye system where one has $\text{FWHM}_{\text{Debye}} = 1.14$ decades. For χ_1'', it is calculated directly from the experimental data. As $|\chi_3^{(3)}|$ is very asymmetric and does not go below 0.5 on the left, we consider only the right part of the hump, and multiply the result by a factor of two, to allow a quantitative comparison with χ_1''. In the insert of Fig. 5(b), we can clearly confirm the similarity of behavior for χ_1'' and $|\chi_3^{(3)}|$. 1-PG has the lowest values of FWHM. There is a jump for $N = 2$ and no noticeable change for $N > 2$.

Finally, the noticeable difference between the first- and third-order spectra lies in the left part of the peak, where we do not detect any sign of the normal mode for the third-order susceptibility, even when inspecting directly the behavior of the imaginary part of the cubic response (not shown). We speculate that this may come from the fact that if the relaxation of a given system is governed by two modes "a" and "b," of respective linear dielectric strength $\Delta\chi_a$ and $\Delta\chi_b$, the relative influences of these two modes is governed by the ratio $\Delta\chi_a/\Delta\chi_b$ for the linear response, but by the square of this ratio for the third-order response. This statement is illustrated by, e.g., Eq. (2). Hence, the small normal mode hardly visible in Fig. 5(a) is not visible on $\chi_3^{(3)}$.

E. Influence of the normal and β modes on the determination of f_α, FWHM, and β_{diel}

We focus our study on the α-relaxation mode. However, higher (β mode,...) and lower (normal mode) frequency relaxation modes are present for the N-PG. In order to see their influence on f_α, FWHM and β_{diel}, the loss experimental spectra have been fitted using three peaks, corresponding to the α, normal,and β modes. In this paragraph, we will refer to

the "total peak" or "total contribution" as the sum of the three HN relaxation peaks: α, β, and normal.

The β mode presents a peak at frequencies higher than our measurement range. It adds a very low contribution to the right wing of the main peak and its influence on f_α, FWHM, and β_{diel} is fully negligible for all the N-PG measured.

Concerning the normal mode, we compared the f_α, FWHM, and β_{diel} of the total and α loss contribution for 20-PG obtained from the maximum of the total and α peaks.

(1) The comparison of the values of f_α shows no difference for $T > 218$ K, the normal mode being very small compared to the α mode. For lower values of T, a difference gradually appears upon cooling for the temperatures in the range 204–218 K. However, the amplitude of this shift remains small; i.e., in the worst case it is not larger than the 0.5 K error bar given for T_g see Sec. IV A 1.

(2) The values of the FWHM from the total and α peaks differ from less than 5%.

(3) The relative difference between the values of β_{diel} from the total and α contributions is less than 0.3%.

(4) In Fig. 5(a), the left wing of the loss peak and moreover the derivative of the loss peak clearly show the emergence of the normal mode for N= 20. For $N = 12$, it was not reasonably possible to introduce a normal peak as the left part of the loss signal was well fitted by a single α contribution.

From these considerations, we conclude that in our experimental conditions, there is no influence of the normal mode on the determination of f_α, FWHM, and β_{diel} for N-PG with $N < 20$. For 20-PG, the normal mode is clearly visible but induces modifications that are small enough to be neglected. This legitimates the calculation of these three parameters directly from of the measured global peak.

F. Relative evolution of N_{corr} in τ_α

Equation (2) shows [12,13] that the temperature dependence of the mean number of molecules in a DH, N_{corr}, can be extracted from that of $\chi_3^{(3)}$, provided that we move to the dimensionless cubic susceptibility $X_3^{(3)}$ defined as

$$X_3^{(3)}(\omega, T) \equiv \frac{\chi_3^{(3)}(\omega, T) k_B T}{\epsilon_0 \, \Delta\chi_1^2 \, a^3},$$

$$X_3^{(3)}(\omega, T) = N_{\text{corr}}(T)\, \mathcal{H}(\omega\tau_\alpha(T)) + X_{3,\text{triv}}^{(3)}(\omega\tau_\alpha(T)), \quad (8)$$

where the definition of $X_3^{(3)}$ shows that its spectrum at each given T can be deduced from that of $\chi_3^{(3)}$ by using only experimentally well-known quantities, and where the last equality arises only when assuming that the Bouchaud-Biroli's prediction holds. $X_{3,\text{triv}}^{(3)}$ is the trivial contribution that would exist even for independent dipoles and which is known from theoretical literature (see Refs. [16,33,38,58,59]). Importantly, the scaling function $\mathcal{H}(\omega\tau_\alpha(T))$ is predicted not to depend explicitly on T, but may depend on the considered liquid, and thus may depend on N. To circumvent this issue of the unknown scaling function, we consider a given value $u_0 = \omega\tau_\alpha$ and normalize the value obtained for $|X_3^{(3)}(u_0) - X_{3,\text{triv}}^{(3)}(u_0)|$ at any temperature by its corresponding value at a reference temperature T_{ref}. As a result, the unknown value of $|\mathcal{H}(u_0)|$ simplifies and one obtains directly $N_{\text{corr}}(T)/N_{\text{corr}}(T_{\text{ref}})$. In practice, we consider the peak of $|X_3^{(3)}|$, for which $u_0 = \omega_p\tau_\alpha = 2\pi f_p\tau_\alpha$,

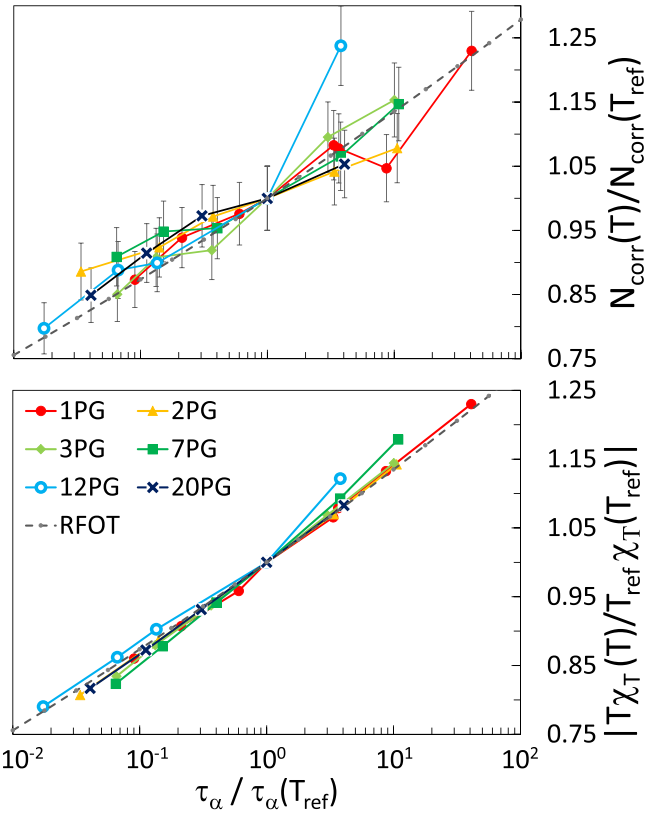


FIG. 6. For all the measured oligomers N-PG ($N = 1, 2, 3, 7, 12, 20$). (a) Relative evolution of the mean number of correlated elements N_{corr} in a dynamic heterogeneity as a function of the relaxation time τ_α. Both N_{corr} and τ_α are normalized by their values at a reference temperature T_{ref}, in order to get rid of the contribution of the unknown $\mathcal{H}$ function. (b) Same kind of plot as in panel (a) but for $T\chi_T(T)$ normalized to its value at T_{ref} to remove the unknown numerical prefactor relating $N_{\text{corr,T}}$ and $T\chi_T$. The gray dashed line represents the RFOT prediction [see Eq. (13)]. Both panels (a) and (b) show that the relative evolution of N_{corr} in τ_α is the same for all values of N varying from 1 to 20 and is very similar to the RFOT prediction, on a wide four-decade range of τ_α.

we draw $X_{3,\text{triv}}^{(3)}(u_0)$ from literature—see Refs. [33,38]—and we select for each N-PG a reference temperature T_{ref} for which $f_\alpha \approx 10$ Hz (see Table II). Figure 6(a) shows the evolution of $N_{\text{corr}}(T)/N_{\text{corr}}(T_{\text{ref}})$ as a function of the relaxation time $\tau_\alpha(T)/\tau_\alpha(T_{\text{ref}})$.

Figure 6 shows that the increase of $N_{\text{corr}}(T)/N_{\text{corr}}(T_{\text{ref}})$ upon cooling is identical, within the error bars, for all the oligomers measured, with N rising from 1 to 20. As we shall discuss in detail in the next section, this was not obvious a priori and represents the key result of this work.

To reinforce this result, let us consider another estimation of N_{corr} drawn from the linear spectra by derivation of τ_α vs T. As it was shown in Refs. [60–62], this estimator $N_{\text{corr,T}}(T)$ is given by

$$N_{\text{corr,T}}(T) \propto T\,\chi_T(T) = \left|\frac{\partial Ln(\tau_\alpha/\tau_0)}{\partial Ln(T)}\right| = T\frac{D\,T_0}{(T - T_0)^2}, \quad (9)$$

where the proportionality factor relating $N_{\mathrm{corr,T}}(T)$ and $T\chi_{\mathrm{T}}$ does not depend on T, even if its precise value is unknown. Once again, this can be circumvented by considering the ratio $\frac{N_{\mathrm{corr,T}}(T)}{N_{\mathrm{corr,T}}(T_{\mathrm{ref}})}$, which is plotted in Fig. 6(b) and reads

$$\frac{N_{\mathrm{corr,T}}(T)}{N_{\mathrm{corr,T}}(T_{\mathrm{ref}})} = \frac{T\chi_{\mathrm{T}}(T)}{T_{\mathrm{ref}}\chi_{\mathrm{T}}(T_{\mathrm{ref}})}. \tag{10}$$

We note that the six liquids studied in the present work are in agreement with the previous works of the Augsburg team—see Refs. [15,54,55] reporting the behavior of $|X_3^{(3)}(\omega\tau_\alpha)|$ in temperature of five different glassformers. In these references, it was shown that the maximum over frequency of the dimensionless cubic susceptibility $|X_3^{(3)}(\omega_{\mathrm{p}}\tau_\alpha)|$ scales in temperature as $E_{\mathrm{act}}(T) \equiv |\partial \ln(\tau_\alpha(T))/\partial(1/T)|$. Because one has $E_{\mathrm{act}}(T) = T \times |T\chi_{\mathrm{T}}|$, and because the cubic response experiments can be followed on a quite narrow interval in temperature $[T_{\mathrm{min}}; T_{\mathrm{max}}]$ with $T_{\mathrm{max}} \simeq 1.15 \times T_{\mathrm{min}}$, the difference between our Fig. 6(a) and the results of Refs. [15,54,55] is below the experimental resolution.

Summarizing, Figs. 6(a) and 6(b) show very similar results. We have two independent estimators of N_{corr}, the first one obtained from the 3ω measurements, the second one from the linear measurements. Both give similar results: The evolution of N_{corr} as a function of τ_α is independent of N. This is a remarkable result, since the two quantities plotted in Figs. 6(a) and 6(b) come from independent lines of thought. We shall now discuss what this implies for our understanding of the glass transition.

IV. DISCUSSION

In Fig. 6, although N varies considerably—from 1 to 20—the behavior remains quantitatively the same. As explained above, because the size of our longest oligomer (presumably) exceeds that of typical dynamic heterogeneities, this result was far from obvious *a priori*, and it establishes that the relative evolution of $N_{\mathrm{corr}}(\tau_\alpha)$ is insensitive to the backbone linking the monomers. Besides, as we show now, many of the quantities often used to characterize glassformers around T_{g} vary in our N range. We shall enumerate them to get a deeper understanding of the meaning of Fig. 6. Finally, we shall inspect what are the predictions of the first-principles theories of the glass transition that we can compare to Fig. 6(a).

A. Microscopic parameters having no impact on Fig. 6

1. Fragility, glass transition temperature, and spectral width

Figure 7 presents the evolution in N of two parameters widely used to classify glassformers, namely, the glass transition temperature T_{g} (blue curve, blue dots, left vertical scale) and fragility m (red curve, red triangles, right vertical scale). Both show a very rapid growth between $N = 1$ and 2, and a slower increase between $N = 2$ and $\approx$6, before reaching a plateau. We have a similar behavior for a third widely used parameter, namely, the stretching, given by χ_1's FWHM (Fig. 5): We can see a jump between $N = 1$ and 2, and a constant value for larger N. Note that the value of T_{g} for 2-PG, situated higher than the curve, has already been reported in Ref. [32]. Overall, despite the noticeable variations of all these three parameters within our range in N, the content of Fig. 6 remains unchanged.

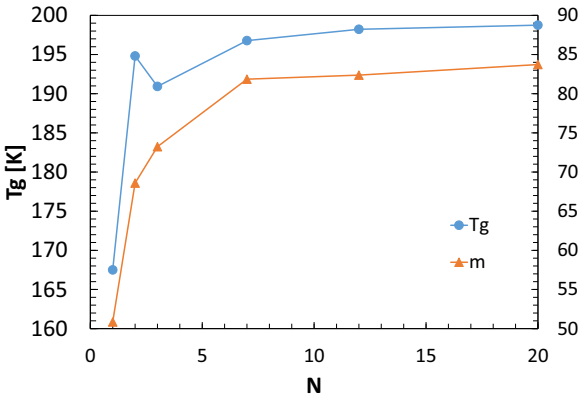


FIG. 7. Glass transition temperatures T_{g} (blue curve, blue dots, and left vertical scale) and fragility m (red curve, red triangles, and right vertical scale) vs N. The error bar on T_{g} is on the order of ± 0.5 K, yielding the relative error on m to be close to $\pm 3\%$.

2. β and other relaxation modes

As detailed in Refs. [32,49], in addition to the α-relaxation mode, there are other modes in N-PG, in particular the β mode, which varies significantly in our range of N. We note that this evolution of the β-relaxation mode does not affect the behavior in Fig. 6. This can be understood because this β-relaxation mode appears at frequencies much higher than f_α, and has a small amplitude. As our frequency experimental range does not extend close to f_β, we shall not enter in the interpretation of nonlinear susceptibility around f_β, which has already been reviewed in Refs. [33,54].

3. Densities of OH bonds and strength of dipole-dipole interactions

As shown in Fig. 8, in our range of N, the numerical density of OH groups varies by a factor $\approx$15. This implies that the OH bonds, which are numerous for $N = 1$, are no longer at play for $N = 20$. Similarly, the dielectric strength $\Delta\chi_1$ varies by a factor 12−14 for our N-PG series, which implies a drastic change for the typical dipole-dipole interaction $\mathcal{I} = \mu^2/(4\pi\epsilon_0 a^3)$ for neighboring dipoles μ separated by a distance a. It is of interest to compare $\mathcal{I}$ to the mean thermal energy per degree of freedom $k_{\mathrm{B}}T_{\mathrm{g}}$ by defining the ratio $R = \mathcal{I}/(k_{\mathrm{B}}T_{\mathrm{g}})$. Remembering that the dielectric strength is given by $\Delta\chi_1 = \mu^2 g_{\mathrm{K}}/(3\epsilon_0 k_{\mathrm{B}} T a^3)$, we get $R \simeq \Delta\chi_1(T_{\mathrm{g}})/(4g_{\mathrm{K}})$, which allows to assess the dependence of R in N. Indeed, with $g_{\mathrm{K}}(N = 1) \simeq 2.85$—see Ref. [53]—we get $R(N = 1) \approx 5$, while $R(N = 20) \overset{<}{\approx} 1$—for the latter case we took $g_{\mathrm{K}}(N = 20) \overset{>}{\approx} 1$ because $\Delta\chi_1(N = 20)$ is very small with respect to $\Delta\chi_1(N = 1)$. Finally, as for the OH bondings, we get that, in our N range, the typical dipole-dipole interaction, scaled by $k_{\mathrm{B}}T_{\mathrm{g}}$, disappears of the game for $N = 20$, while it is non-negligible *a priori* for $N = 1$. Yet, neither of these two qualitative changes has any consequence in Fig. 6.

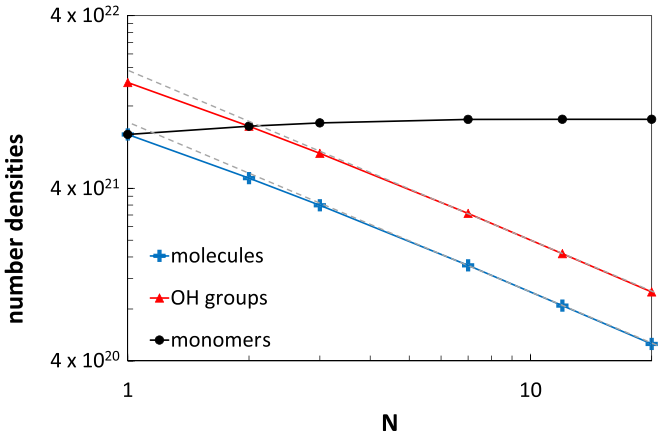


FIG. 8. Number of molecules, monomers and –OH groups per cm^3 obtained from the densities given by the suppliers, varying from $\simeq$1.036 to 1.00 g/cm^3 for $N = 1-20$. Apart from the simple behavior (constant or $\propto 1/N$), there is a slight bending for the range $1 \leqslant N \leqslant 3$, which could contribute to the variations of T_g and m for $N \leqslant 3$.

B. Prediction of the various first-principles theories of the glass transition for Fig. 6

We now move to a comparison with theoretical predictions. We limit ourselves to discuss theoretical frameworks constructed to account for the glass transition in itself. We leave aside the various phenomenological models taking the viscous slowdown for granted and attempting to model the cubic nonlinear responses. As shown in Ref. [13], most of these models (if not all) implicitly require the growth of dynamically correlated domains upon cooling, and are consistent with the general prediction of Bouchaud and Biroli expressed in Eq. (2).

1. Random first-order transition theory

RFOT is a first-principles theory of glass formation inspired by *p*-spin models [63]. Its main output is that the physics of supercooled liquids is driven by the emergence of amorphous order, i.e., by nonperiodic configurations of very low free energy [18,64–67]. The typical size ξ_{stat} of these amorphously ordered domains—called glassites—increases upon cooling, because of the decrease of the configurational entropy $s_c(T)$ with T. As a result, upon cooling, the free energy term $\propto s_c(T)\xi_{stat}^3$, pushing any glassite to "melt," i.e., to change its amorphously ordered configuration, needs larger values of ξ_{stat} to counterbalance the "pinning" free energy term $\propto \xi_{stat}^{3/2}$ which, because of boundary conditions, pushes the glassite to remain in its amorphously ordered initial configuration [18,64–67].

In RFOT, $\xi_{stat}(T)$ is *a priori* different from the dynamical correlation length $\xi_{dyn}(T)$ obtained from the four points correlation function defining the size of DHs, and on general grounds $\xi_{stat} \leqslant \xi_{dyn}$. In practice, as the dynamics is driven by the glassites themselves [64], ξ_{stat}/ξ_{dyn} is a constant of order one close to T_g, and RFOT states [18,66,67] that the number

TABLE III. Calculation of the crossover value $N^\star$ within RFOT: The ΔC_p values are from Ref. [68] and must be converted in J/(mole.K) before using Eq. (12) to get the number of beads per oligomer. As the density of *N*-PG is—mainly—independent of N, the decrease of ΔC_p when N increases explains why the number of beads per oligomer increases much less than linearly in N—fourth column. This finally leads to a number of monomer per DH increasing with N—last columns.

N	ΔC_p J/(g K)	m	n_{beads} per oligomer	$n_{oligomer}$ per DH	N_{mono} per DH	$N^\star$ from Eq. (3) with prefactor $= 0.9$	or	$= 1.8$
1	0.87	51	4.4	43.9	43.9	4.9	or	9.8
3	1.07	77	9.0	21.6	65	5.9	or	11.8
7	0.70	82	12.4	15.7	110	7.5	or	15
17	0.64	84	26.2	7.45	127	8.0	or	16.0
34	0.600	84	48.7	4.00	136	8.2	or	16.4
68	0.556	84	90.0	2.17	147	8.5	or	17.0

N_{corr} of correlated beads is given by

$$N_{corr}(T) = \left[\frac{8}{3\sqrt{3\pi}} \frac{\ln(\tau_\alpha(T)/\tau_0)}{\ln(\alpha_L a^2/(\pi e))}\right]^2, \tag{11}$$

with τ_0 the microscopic time defined above in Eq. (4); a the size of a bead, i.e., the size of an effective degree of freedom deduced from the molecular latent heat of crystallization; and $\alpha_L \simeq (10/a)^2$ the effective Einstein oscillator force constant acting on a bead. Reference [69] gives the definition of beads, as well as the number of beads per oligomer n_{beads}, provided that the fragility m and the specific heat jump per mole ΔC_p are known:

$$n_{beads} = \frac{34.7 \times \Delta C_p}{m \times S_{LJ}} \quad \text{with} \quad S_{LJ} = 1.68\ k_B \simeq 10\ \text{J/mole}. \tag{12}$$

Because in Eq. (11), the dependence on microscopic parameters is only logarithmic, and because $\tau_\alpha(T_g)/\tau_0$ is so large, one of the RFOT's prediction [18,66,67] is that the number of correlated beads is a quasiuniversal number $\simeq 195$ at T_g. Table III shows that, by using the data measured by Johari *et al.* [68] we can draw from Eq. (12) the number of beads per oligomer, given in the fourth column of Table III. By using the RFOT prediction that 195 beads are dynamically correlated at T_g, one finds the number of oligomers contained in any typical DH at T_g (see the fifth column of Table III). By multiplying this result by N, we find the number "N_{mono} per DH" of monomers contained in a DH at T_g (see the sixth column of Table III). Finally, this result can be inserted in the right-hand side of Eq. (3) to get the sought value of $N^\star$, which value depends of the chosen prefactor in Eq. (3), i.e., on whether one compares the DH diameter to R_{ee} of to D_{sph}. A self-consistent analysis of the last column of Table III shows that $N^\star \simeq 16$ in the former case, while $N^\star \simeq 7$ in the latter case. We shall discuss briefly these values in the conclusion.

We now use Eq. (11) to get the RFOT prediction relevant for our experimental Fig. 6. We get

$$\left[\frac{N_{corr}(T)}{N_{corr}(T_{ref})}\right]_{RFOT} = \left[1 + \frac{\ln(\tau_\alpha(T)/\tau_\alpha(T_{ref}))}{\ln(\tau_\alpha(T_{ref})/\tau_0)}\right]^2, \tag{13}$$

which implies that the experimental quantities plotted in Fig. 6 (1) should fall down onto a master curve—owing to the logarithmic dependence in τ_0 and (2) that this master curve should be indistinguishable from a straight line if the experimental resolution is $\pm 5\%$ as in our Fig. 6(a)—owing to the fact that the ratio of logs is smaller than 0.16 in absolute value. Both features are observed in Fig. 6, where the RFOT prediction is plotted as a dashed black line, showing that RFOT is quantitatively consistent with our experimental behavior.

2. Frustration theory

Frustration theory is another first-principle framework [70] making the assumption that a locally preferred structure (LPS), maximizing the local density, plays the key role around the crystallization temperature T_m. Frustration comes in because this LPS cannot tile the three-dimensional space [70]. Upon cooling, the viscous slowing down arises because of the growth of the size ξ_{LPS} of LPS domains surrounded by defects that cost energy. It turns out that general predictions can be done [70] by mapping the problem to the abstract space $\mathcal{E}$ which metrics is curved just enough to allow the LPS crystallizing at a temperature $T^\star$. One distinctive general prediction is that, even though ξ_{LPS} grows upon cooling below $T_m \leqslant T^\star$, there is a low temperature T_{sat} below which ξ_{LPS} saturates, because frustration is so strong that there is no way to further optimize the free energy. As a result, τ_α is predicted to recover a simply activated behavior below T_{sat}.

Frustration theory is thus really different from RFOT, where one predicts that ξ_{stat} diverges at the Kauzmann temperature $T_K < T_g$. However, even if some detailed calculations exist in model systems [71,72], predictions in realistic cases are limited in Frustration theory, mainly because the nature of the LPS is unknown and may depend on molecular details—the only known case is that of liquids of spheres, for which the LPS is an icosahedron [70]. As $\tau_\alpha(T)$ remains superactivated at least down to T_g, T_{sat} must be below T_g, i.e., nonlinear experiments below T_{sat} would be extremely long and difficult. Moreover, as LPS—assuming that they exist—are extremely complicated molecular arrangements, they may well couple to the applied field in a way very similar to that of amorphously ordered glassites put forward by RFOT. Indeed, we shall advocate in the next section that the crucial point to account for nonlinear experiments is that collective effects play the central role, which, as we shall argue, is much more a demanding requirement than mere dynamical correlations. These collective effects amount to get some molecular configurations which, because they have a low value of free energy, react collectively to the applied field, because of the rigidity that is the counterpart of their collective optimization.

To conclude our comparison of Frustration theory predictions with our Fig. 6, it is possible that this theory is consistent with our data, but we cannot push our experiments in the range where the distinctive features of Frustration with respect to RFOT can be inspected, consistently to what some of us had already discussed in Ref. [38].

3. Kinetically constrained models

Kinetically constrained models (KCM) are a family of models [73–76] assuming that the thermodynamics of supercooled liquids is trivial, i.e., that the Hamiltonian $\mathcal{H}$ boils down to that of an ideal gas of particles, and that the nontrivial dynamical rules only matter to account for all the glass phenomenology around T_g. At first sight, this may seem strange, since one may ask how nontrivial dynamical rules may arise when the hamiltonian is trivial? This is nonetheless possible, as it has been analytically demonstrated on the so-called plaquettes models [77,78]: To give a simple illustration, consider a two-dimensionnal space tiled with, e.g., triangular plaquettes [77], each containing three physical spins S_{i_1}, S_{i_2}, and S_{i_3} at its vertex. Then, assume that each physical spin interacts exclusively with the two other spins of the same plaquette i. This Hamiltonian $\mathcal{H}(\{S_{i_k} = \pm 1\})$ is complicated, since each spin belongs to the two plaquettes that it connects. However, it was demonstrated that this Hamiltonian can be mapped to another one involving only the plaquettes variables $\sigma_i = S_{i_1} S_{i_2} S_{i_3}$, and that $H(\{\sigma_i\}) = \Sigma_i \sigma_i$, i.e., we have a trivial "ideal gaz" of plaquettes variables. As for the dynamical rules [77] of the plaquettes variables σ_i, they are the result of the thermal fluctuations of the physical spins S_{i_k}: It turns out that these rules are complex, since the ability of σ_i to relax to its lowest energy state depends on the state of its neighboring plaquette variables. This flip may happen only in the case where at least one of the neighboring plaquette variable is in its excited state. This is a quantitative illustration of the key intuition of the KCM models [74]: As the excited states $\sigma_i = 1$ are rare at low T, they can be thought as "empty sites," i.e., sites where the free volume lies. As a result, it is physically very appealing that relaxation around T_g only happens in the sites having at least one empty neighbor (i.e., a neighbor where $\sigma = 1$). Besides, as the average concentration c_{exc} of empty sites is very small at low T, this creates long relaxation time [79,80] as regions containing as much as $1/c_{exc}$ sites have to "share" the same excitation; i.e., the full relaxation of the region will be over only when the same elementary piece of free volume will have come around each site. Finally, as $c_{exc} \ll 1$, one naturally expects [74,80] strong spatial heterogeneties of the dynamics: The faster regions are those which, at a given time, are richer than the average in empty sites. To summarize, KCM models naturally account [73,76] for the main features of glassy dynamics around T_g.

Do KCM models account for the nonlinear response behavior such as those shown in Figs. 4 and 6(a)? This question is still debated and opposite views coexist in the literature [38,52,81–83]. The difficulty lies in the fact that there is no analytical way to derive explicitly cubic responses $\chi_3(\omega, T)$ starting only from an expression of $\mathcal{H}$ as given by KCM models. Some works claim [82,83] that, starting from the main KCM ideas, one can cook equations accounting—semiquantitatively—for the experimental behavior of cubic responses. On the other hand, some general arguments have concluded in the opposite way [38,52]. Importantly, a recent numerical work [81], in which one of us is involved, simulates explicitly a very simple KCM model and finds that its cubic responses $\chi_{3,KCM}(\omega, T)$ do not show the main experimental features: $|\chi_{3,KCM}(\omega, T)|$ has no peak at finite frequency and decreases monotonously when increasing the frequency; besides, the dimensionless cubic susceptibility $|X_{3,KCM}(\omega, T)|$ is strictly independent of T when plotted as a function of $\omega\tau_\alpha$. This is at odds of our Figs. 4 and 6(a).

How is it possible that a KCM model, as that of Ref. [81], is able at the same time to account for dynamical heterogeneities and not for the nonlinear behavior? As explained in Ref. [81], this comes from the difference between dynamical correlation effects and genuine collective effects. Collective effects arise when it exists some molecular configurations $\mathcal{C}_{\rm opt}$ of low free energy $\mathcal{F}_{\rm opt}$, i.e., preferred configurations where the interactions between $\approx N_{\rm corr}$ molecules lead to a significant lowering of $\mathcal{F}$. Even if such preferred configurations are aperiodic, even if they do not yield the absolute minimum of $\mathcal{F}$, even if they only involve a finite value of $N_{\rm corr}$, there is, nonetheless, a trend to come back to such preferred configurations when the system is submitted to an external field. Because a configuration $\mathcal{C}_{\rm opt}$ arises by efficiently combining interactions between $\approx N_{\rm corr}$ molecules, the coupling to an external field will be larger for larger $N_{\rm corr}$, yielding finally an overall behavior of $|\chi_3^{(3)}|$ tracking that of $N_{\rm corr}$. In a KCM model, however, one starts by assuming that the value of $\mathcal{F}$ negligibly depends on the considered configuration [73,76]: Therefore, there is no trend to come back to any configuration, and, within a given DH of $N_{\rm corr}$ molecules, the field couples only to one molecule at a time, namely, the one having the opportunity to relax because it has an empty neighbor. Hence, the overall behavior where $|\chi_3^{(3)}(\omega\tau_\alpha)|$ is a constant in temperature, as in any noninteracting model.

Therefore, despite its extremely simplified character, the KCM model of Ref. [81] has the great interest of giving an example where Fig. 6(a) cannot be accounted for—as just explained—while Fig. 6(b) can be accounted for. Indeed, because it involves only $\ln(\tau_\alpha(T))$ and its derivative in temperature, Fig. 6(b) is recovered by any model accounting well enough for the behavior of $\ln(\tau_\alpha(T))$. This illustrates that $\chi_3(\omega, T)$ and $N_{\rm corr,T}$ come from distinct lines of thought, as already emphasized (see Refs. [30,62]). The fact that the overall behavior of Figs. 6(a) and 6(b) is very similar is thus an extremely nontrivial result and a strong argument in favor of thermodynamic theories stating that order effects—either amorphous or LPS driven—play a key role in the glass transition.

V. CONCLUSION

We performed linear and 3ω dielectric measurement on a family of oligomers, N-PG, with N ranging from 1 to 20, in order to investigate the influence of the length of the chain on the glass transition properties. The parameters obtained from our linear measurements are in good agreement with those reported in previous results [31,32,48,49]. The influence of N on the basic properties such as $T_{\rm g}$ and m is clear for $N \leqslant 3$, but is marginal as soon as $N > 3$.

We showed that the dielectric linear susceptibility $\Delta\chi_1$ varies as $1/N$. As the possible variation of the Kirkwood factor with N is far from explaining this effect, the simplest interpretation would be to imagine that the only contribution to the polarization would be due to the two ending OH groups, no other contribution coming, in our measurement conditions, from the chemical units situated in-between. In this scenario, varying the length of the molecule from 1 to 20, we do not perturb the dipoles. This is an unexpected and nonobvious behavior, which has not yet received its microscopic justification.

With a molecule length extending from 1 to 20, our MD simulations allow to know that we explore either side of the DH mean diameter $D_{\rm corr}$ close to $T_{\rm g}$. We naturally expected a modification of the evolution of characteristic parameters around $D_{\rm corr}$, like the fragility m, $T_{\rm g}$ or even the relative evolution of $N_{\rm corr}$ in temperature. To locate precisely this crossover, the difficultly lies in predicting the absolute value of $D_{\rm corr} \propto N_{\rm corr}^{1/3}$ for which very different experimental estimates coexist in the literature. We note however that within RFOT, we come to a prediction that the crossover is expected for N-PG chains of length $N^\star(\tau_\alpha = 10\,{\rm ms}) \simeq 7$, which amounts, by the same reasoning, to $N^\star(\tau_\alpha = 100\,{\rm s}) \simeq 8.4$. This is nearly three times larger than the characteristic chain length $\approx$3 beyond which $T_{\rm g}(N)$ and $m(N)$ no longer evolve, as observed in Fig. 7. But it is difficult to disentangle the various effects, as $T_{\rm g}$ and m are also correlated to the volume density of monomers.

In contrast, the absence of influence of the chain length in Fig. 6 is striking. Using two independent estimators, which reinforce each other, we showed that the relative evolution of $N_{\rm corr}$ versus T is independent of N. Consequently, the results presented in Fig. 6 depend neither on $T_{\rm g}$, nor on m, nor on the spectral width, nor on the β-relaxation intensity, nor on the volumic density of H bonds, nor of the strength of dipole-dipole interactions, nor on the length of the chain, even when we approach the crossover value $N^\star$ introduced in this work, where one may have expected an effect of the molecular skeleton. Thus, this plot unveils a very robust property close to the glass transition. Besides, as discussed above, Fig. 6(a) is of great physical interest since it cannot be accounted for by some of the first-principles theories of the glass transition, at variance with Fig. 6(b).

ACKNOWLEDGMENTS

We warmly thank Nicolas Delpouve for long-term collaboration and Marceau Hénot for his introduction to numerical methods in open-source Molecular Dynamics software. Besides, we acknowledge financial support by IRAMIS, as well as by the French Government under the France 2030 program, reference ANR-11-IDEX-003 (Interglass Project of the PHOM Department of University Paris-Saclay), and by Agence Nationale de la Recherche, reference ANR-24-CE30-0442 (GLASSGO project).

DATA AVAILABILITY

The data that support the findings of this article are not publicly available. The data are available from the authors upon reasonable request.

[1] L. Berthier and G. Biroli, Theoretical perspective on the glass transition and amorphous materials, Rev. Mod. Phys. **83**, 587 (2011).

[2] A. Cavagna, Supercooled liquids for pedestrians, Phys. Rep. **476**, 51 (2009).

[3] O. Dauchot, F. Ladieu, and C. P. Royall, The glass transition in molecules, colloids and grains: Universality and specificity, C. R. Phys. **24**, 25 (2023).

[4] P. G. Debenedetti and F. H. Stillinger, Supercooled liquids and the glass transition, Nature (London) **410**, 259 (2001).

[5] M. D. Ediger, Spatially heterogeneous dynamics in supercooled liquids, Annu. Rev. Phys. Chem. **51**, 99 (2000).

[6] R. Richert, Heterogeneous dynamics in liquids: Fluctuations in space and time, J. Phys.: Condens. Matter **14**, R703 (2002).

[7] R. Richert, N. Israeloff, C. Alba-Simionesco, F. Ladieu, and D. L'Hôte, Experimental approaches to heterogeneous dynamics, in *Dynamical Heterogeneities in Glasses, Colloids, and Granular Media*, edited by L. Berthier, G. Biroli, J.-P. Bouchaud, L. Cipelletti, and W. V. Saarloos, International Series of Monographs on Physics (Oxford University Press, New York , 2011), pp. 152–202.

[8] M. M. Hurley and P. Harrowell, Kinetic structure of a two-dimensional liquid, Phys. Rev. E **52**, 1694 (1995).

[9] C. Scalliet, B. Guiselin, and L. Berthier, Thirty milliseconds in the life of a supercooled liquid, Phys. Rev. X **12**, 041028 (2022).

[10] E. V. Russell and N. E. Israeloff, Direct observation of molecular cooperativity near the glass transition, Nature (London) **408**, 695 (2000).

[11] F. Kremer and A. Schönhals (eds.), *Broadband Dielectric Spectroscopy* (Springer, Berlin, 2003).

[12] J.-P. Bouchaud and G. Biroli, Nonlinear susceptibility in glassy systems: A probe for cooperative dynamical length scales, Phys. Rev. B **72**, 064204 (2005).

[13] P. Gadige, S. Albert, M. Michl, Th Bauer, P. Lunkenheimer, A. Loidl, R. Tourbot, C. Wiertel-Gasquet, G. Biroli, J.-P. Bouchaud, and F. Ladieu, Unifying different interpretations of the nonlinear response in glass-forming liquids, Phys. Rev. E **96**, 032611 (2017).

[14] C. Crauste-Thibierge, C. Brun, F. Ladieu, D. L'Hôte, G. Biroli, and J.-P. Bouchaud, Evidence of growing spatial correlations at the glass transition from nonlinear response experiments, Phys. Rev. Lett. **104**, 165703 (2010).

[15] Th Bauer, P. Lunkenheimer, and A. Loidl, Cooperativity and the freezing of molecular motion at the glass transition, Phys. Rev. Lett. **111**, 225702 (2013).

[16] R. Casalini, D. Fragiadakis, and C. M. Roland, Dynamic correlation length scales under isochronal conditions, J. Chem. Phys. **142**, 064504 (2015).

[17] E. Thoms and R. Richert, A "hump" in the third-order dielectric response of a highly polar liquid: Now you see it, now you don't, J. Chem. Phys. **162**, 114501 (2025).

[18] A. R. Young-Gonzales, K. Adrjanowicz, M. Paluch, and R. Richert, Nonlinear dielectric features of highly polar glass formers: Derivatives of propylene carbonate, J. Chem. Phys. **147**, 224501 (2017).

[19] K. Moch, C. Gainaru, and R. Böhmer, Dielectric and shear-mechanical "humps" in the nonlinear response of polar glassformers, J. Phys. Chem. B **128**, 8846 (2024).

[20] G. Diezemann, Nonlinear response theory for Markov processes: Simple models for glassy relaxation, Phys. Rev. E **85**, 051502 (2012).

[21] G. Diezemann, Higher-order correlation functions and nonlinear response functions in a Gaussian trap model, J. Chem. Phys. **138**, 12A505 (2013).

[22] G. Diezemann, Nonlinear response functions in an exponential trap model, J. Non-Cryst. Solids **407**, 61 (2015).

[23] R. Richert and S. Weinstein, Nonlinear dielectric response and thermodynamic heterogeneity in liquids, Phys. Rev. Lett. **97**, 095703 (2006).

[24] B. Schiener, R. Böhmer, A. Loidl, and R. V. Chamberlin, Nonresonant spectral hole burning in the slow dielectric response of supercooled liquids, Science **274**, 752 (1996).

[25] S. Samanta and R. Richert, Dynamics of glass-forming liquids. XVIII. Does entropy control structural relaxation times? J. Chem. Phys. **142**, 044504 (2015).

[26] F. Ladieu, C. Brun, and D. L'Hôte, Nonlinear dielectric susceptibilities in supercooled liquids: A toy model, Phys. Rev. B, **85**, 184207 (2012).

[27] U. Buchenau, Retardation and flow at the glass transition, Phys. Rev. E **93**, 032608 (2016).

[28] *Nonlinear Dielectric Spectroscopy (Advances in Dielectrics)*, edited by R. Richert (Springer International Publishing, Cham, 2018).

[29] T. Ishikawa and A. Teramoto, The dimensions and dipole moments of poly (propylene glycol) chains, Polym. J. **6**, 207 (1974).

[30] G. Allen, C. Booth, and M. N. Jones, Polypropylene oxide II—Dilute solution properties and tacticity, Polymer **5**, 257 (1964).

[31] C. Gainaru and R. Böhmer, Oligomer-to-polymer transition of poly (propylene glycol) revealed by dielectric normal modes, Macromolecules **42**, 7616 (2009).

[32] C. Gainaru, W. Hiller, and R. Bohmer, A dielectric study of oligo-and poly (propylene glycol), Macromolecules **43**, 1907 (2010).

[33] S. Albert, M. Michl, P. Lunkenheimer, A. Loidl, P. M. Déjardin, and F. Ladieu, Third and fifth harmonic responses in viscous liquids, J. Stat. Mech.: Theory Exp. (2019) 124003.

[34] C. Thibierge, D. l' Hôte, F. Ladieu, and R. Tourbot, A method for measuring the nonlinear response in dielectric spectroscopy through third harmonics detection, Rev. Sci. Instrum. **79**, 103905 (2008).

[35] D. A. Case, H. M. Aktulga, K. Belfon, D. S. Cerutti, G. A. Cisneros, V. W. D. Cruzeiro, N. Forouzesh, T. J. Giese, A. W. Götz, H. Gohlke *et al.*, AmberTools, J. Chem. Inf. Model. **63**, 6183 (2023).

[36] P. Eastman, R. Galvelis, R. P. Peláez, C. R. A. Abreu, S. E. Farr, E. Gallicchio, A. Gorenko, M. M. Henry, F. Hu, J. Huang, A. Krämer, J. Michel, J. A. Mitchell, V. S. Pande, J. P. G. L. M. Rodrigues, J. Rodriguez-Guerra, A. C. Simmonett, S. Singh, J. Swails, P. Turner *et al.*, OpenMM 8: Molecular dynamics simulation with machine learning potentials, J. Phys. Chem. B **128**, 109 (2024).

[37] P. Lunkenheimer, A. Loidl, B. Riechers, A. Zaccone, and K. Samwer, Thermal expansion and the glass transition, Nat. Phys. **19**, 694 (2023).

[38] S. Albert, Th Bauer, M. Michl, G. Biroli, J.-P. Bouchaud, A. Loidl, P. Lunkenheimer, R. Tourbot, C. Wiertel-Gasquet, and F. Ladieu, Fifth-order susceptibility unveils growth of thermodynamic amorphous order in glass-formers, Science **352**, 1308 (2016).

[39] S. A. Reinsberg, X. H. Qiu, M. Wilhelm, H. W. Spiess, and M. D. Ediger, Length scale of dynamic heterogeneity in supercooled glycerol near t_g, J. Chem. Phys. **114**, 7299 (2001).

[40] U. Tracht, M. Wilhelm, A. Heuer, H. Feng, K. Schmidt-Rohr, and H. W. Spiess, Length scale of dynamic heterogeneities at the glass transition determined by multidimensional nuclear magnetic resonance, Phys. Rev. Lett. **81**, 2727 (1998).

[41] S. Tatsumi, S. Aso, and O. Yamamuro, Thermodynamic study of simple molecular glasses: Universal features in their heat capacity and the size of the cooperatively rearranging regions, Phys. Rev. Lett. **109**, 045701 (2012).

[42] S. Merabia and D. Long, Heterogeneous dynamics and pressure dependence of the dynamics in van der Waals liquids, Macromolecules **41**, 3284 (2008).

[43] T. C. Merlette, J. Hem, Caroline Crauste-Thibierge, Sergio Ciliberto, Florence Clément, P. Sotta, and Didier R. Long, Theory of plasticity and strain hardening of glassy polymers, Macromolecules **56**, 6510 (2023).

[44] C. Dalle-Ferrier, A. Kisliuk, L. Hong, G. Carini, G. Carini, G. D' Angelo, C. Alba-Simionesco, V. N. Novikov, and A. P. Sokolov, Why many polymers are so fragile: A new perspective, J. Chem. Phys. **145**, 154901 (2016).

[45] G. S. Fulcher, Analysis of recent measurements of the viscosity of glasses, J. Am. Ceram. Soc. **8**, 339 (1925).

[46] G. Tammann and W. Hesse, Die Abhängigkeit der Viscosität von der Temperatur bei unterkühlten Flüssigkeiten, Z. Anorg. Allg. Chem. **156**, 245 (1926).

[47] H. Vogel, Das temperaturabhangigkeitsgesetz der viskosität von flussigkeiten, Phys. Z. **22**, 645 (1921).

[48] C. Gainaru, T. Hecksher, F. Fan, K. Xing, B. Cetinkaya, N. B. Olsen, J. C. Dyre, A. P. Sokolov, and R. Böhmer, Simple-liquid dynamics emerging in the mechanical shear spectra of poly (propylene glycol), Colloid Polym. Sci. **295**, 2433 (2017).

[49] M. Köhler, P. Lunkenheimer, Y. Goncharov, R. Wehn, and A. Loidl, Glassy dynamics in mono-, di-and tri-propylene glycol: From the α-to the fast β-relaxation, J. Non-Cryst. Solids **356**, 529 (2010).

[50] K. L. Ngai, P. Lunkenheimer, C. Leon, U. Schneider, R. Brand, and A. Loidl, Nature and properties of the Johari–Goldstein β-relaxation in the equilibrium liquid state of a class of glass-formers, J. Chem. Phys. **115**, 1405 (2001).

[51] Y. Ding, V. N. Novikov, A. P. Sokolov, A. Cailliaux, C. Dalle-Ferrier, C. Alba-Simionesco, and B. Frick, Influence of molecular weight on fast dynamics and fragility of polymers, Macromolecules **37**, 9264 (2004).

[52] G. Biroli, J.-P. Bouchaud, and F. Ladieu, Amorphous order and nonlinear susceptibilities in glassy materials, J. Phys. Chem. B **125**, 7578 (2021).

[53] T. Böhmer, F. Pabst, J. P. Gabriel, and T. Blochowicz, Dipolar order controls dielectric response of glass-forming liquids, Phys. Rev. Lett. **132**, 206101 (2024).

[54] P. Lunkenheimer, M. Michl, Th Bauer, and A. Loidl, Investigation of nonlinear effects in glassy matter using dielectric methods, Eur. Phys. J. Spec. Top. **226**, 3157 (2017).

[55] M. Michl, Th Bauer, P. Lunkenheimer, and A. Loidl, Nonlinear dielectric spectroscopy in a fragile plastic crystal, J. Chem. Phys. **144**, 114506 (2016).

[56] M. Hénot, P.-M. Déjardin, and F. Ladieu, Orientational dynamics in supercooled glycerol computed from MD simulations: Self and cross contributions, Phys. Chem. Chem. Phys. **25**, 29233 (2023).

[57] M. Hénot and F. Ladieu, Emergence of a hump in the cubic dielectric response of glycerol, Phys. Rev. Lett. **134**, 218202 (2025).

[58] W. T. Coffey and B. V. Paranjape, Dielectric and Kerr effect relaxation in alternating electric fields, Proc. R. Ir. Acad., Sect. A **78**, 17 (1978).

[59] J. L. Déjardin and Y. P. Kalmykov, Nonlinear dielectric relaxation of polar molecules in a strong ac electric field: Steady state response, Phys. Rev. E **61**, 1211 (2000).

[60] L. Berthier, G. Biroli, J.-P. Bouchaud, W. Kob, K. Miyazaki, and D. R. Reichman, Spontaneous and induced dynamic correlations in glass formers. Ii. Model calculations and comparison to numerical simulations, J. Chem. Phys. **126**, 184504 (2007).

[61] L. Berthier, G. Biroli, J.-P. Bouchaud, W. Kob, K. Miyazaki, and D. R. Reichman, Spontaneous and induced dynamic fluctuations in glass formers. I. General results and dependence on ensemble and dynamics, J. Chem. Phys. **126**, 184503 (2007).

[62] C. Dalle-Ferrier, C. Thibierge, C. Alba-Simionesco, L. Berthier, G. Biroli, J.-P. Bouchaud, F. Ladieu, D. L'Hôte, and G. Tarjus, Spatial correlations in the dynamics of glassforming liquids: Experimental determination of their temperature dependence, Phys. Rev. E **76**, 041510 (2007).

[63] T. R. Kirkpatrick, D. Thirumalai, and P. G. Wolynes, Scaling concepts for the dynamics of viscous liquids near an ideal glassy state, Phys. Rev. A **40**, 1045 (1989).

[64] G. Biroli and J.-P. Bouchaud, The RFOT theory of glasses: Recent progress and open issues, C. R. Phys. **24**, 9 (2024).

[65] J.-P. Bouchaud and G. Biroli, On the adam-gibbs-kirkpatrick-thirumalai-wolynes scenario for the viscosity increase in glasses, J. Chem. Phys. **121**, 7347 (2004).

[66] V. Lubchenko and P. G. Wolynes, Theory of structural glasses and supercooled liquids, Annu. Rev. Phys. Chem. **58**, 235 (2007).

[67] X. Xia and P. G. Wolynes, Fragilities of liquids predicted from the random first order transition theory of glasses, Proc. Natl. Acad. Sci. USA **97**, 2990 (2000).

[68] G. P. Johari, A. Hallbrucker, and E. Mayer, Calorimetric relaxation and glass transition in poly (propylene glycols) and its monomer, J. Polym. Sci., Part B:Polym. Phys. **26**, 1923 (1988).

[69] J. D. Stevenson and P. G. Wolynes, Thermodynamic-kinetic correlations in supercooled liquids: A critical survey of experimental data and predictions of the random first-order transition theory of glasses, J. Phys. Chem. B **109**, 15093 (2005).

[70] G. Tarjus, S. A. Kivelson, Z. Nussinov, and P. Viot, The frustration-based approach of supercooled liquids and the glass transition: A review and critical assessment, J. Phys.: Condens. Matter **17**, R1143 (2005).

[71] F. Sausset, G. Tarjus, and P. Viot, Tuning the fragility of a glass-forming liquid by curving space, Phys. Rev. Lett. **101**, 155701 (2008).

[72] F. Sausset, G. Tarjus, and P. Viot, Thermodynamics and structure of simple liquids in the hyperbolic plane, J. Stat. Mech.: Theory Exp. (2009) P04022.

[73] D. Chandler and J. P. Garrahan, Dynamics on the way to forming glass: Bubbles in space-time, Annu. Rev. Phys. Chem. **61**, 191 (2010).

[74] G. H. Fredrickson and H. C. Andersen, Facilitated kinetic Ising models and the glass transition, J. Chem. Phys. **83**, 5822 (1985).

[75] L. O. Hedges, R. L. Jack, J. P. Garrahan, and D. Chandler, Dynamic order-disorder in atomistic models of structural glass formers, Science **323**, 1309 (2009).

[76] F. Ritort and P. Sollich, Glassy dynamics of kinetically constrained models, Adv. Phys. **52**, 219 (2003).

[77] J. P. Garrahan, Glassiness through the emergence of effective dynamical constraints in interacting systems, J. Phys.: Condens. Matter **14**, 1571 (2002).

[78] R. M. Turner, R. L. Jack, and J. P. Garrahan, Overlap and activity glass transitions in plaquette spin models with hierarchical dynamics, Phys. Rev. E **92**, 022115 (2015).

[79] R. L. Jack and J. P. Garrahan, Caging and mosaic length scales in plaquette spin models of glasses, J. Chem. Phys. **123**, 164508 (2005).

[80] A. C. Pan, J. P. Garrahan, and D. Chandler, Heterogeneity and growing length scales in the dynamics of kinetically constrained lattice gases in two dimensions, Phys. Rev. E **72**, 041106 (2005).

[81] E. Bertin and F. Ladieu, Nonlinear dielectric response in glass formers: Restoring forces and avoided spin-glass criticality, Phys. Rev. E **109**, 064156 (2024).

[82] T. Speck, Dynamic facilitation theory: A statistical mechanics approach to dynamic arrest, J. Stat. Mech. (2019) 084015.

[83] T. Speck, Modeling non-linear dielectric susceptibilities of supercooled molecular liquids, J. Chem. Phys. **155**, 014506 (2021).